FULLY COUPLED SIMULATIONS OF NON-COLLOIDAL MONODISPERSE SHEARED SUSPENSIONS

M. Abbas[1], E. Climent[1,*] and O. Simonin[2]

[1]**Laboratoire de Génie Chimique, Toulouse, France.**
[2]**Institut de Mécanique des Fluides, Toulouse, France.**

Abstract: In this work we investigate numerically the dynamics of sheared suspensions in the limit of vanishingly small fluid and particle inertia. The numerical model we used is able to handle the multi-body hydrodynamic interactions between thousands of particles embedded in a linear shear flow. The presence of the particles is modelled by momentum source terms spread out on a spherical envelop forcing the Stokes equations of the creeping flow. Therefore all the velocity perturbations induced by the moving particles are simultaneously accounted for.

The statistical properties of the sheared suspensions are related to the velocity fluctuation of the particles. We formed averages for the resulting velocity fluctuation and rotation rate tensors. We found that the latter are highly anisotropic and that all the velocity fluctuation terms grow linearly with particle volume fraction. Only one off-diagonal term is found to be non zero (clearly related to trajectory symmetry breaking induced by the non-hydrodynamic repulsion force). We also found a strong correlation of positive/negative velocities in the shear plane, on a time scale controlled by the shear rate (direct interaction of two particles). The time scale required to restore uncorrelated velocity fluctuations decreases continuously as the concentration increases. We calculated the shear induced self-diffusion coefficients using two different methods and the resulting diffusion tensor appears to be anisotropic too.

The microstructure of the suspension is found to be drastically modified by particle interactions. First, the probability density function of velocity fluctuations showed a transition from exponential to Gaussian behaviour as particle concentration varies. Second, the probability of finding close pairs while the particles move under shear flow is strongly enhanced by hydrodynamic interactions when the concentration increases.

Keywords: hydrodynamic interactions; force coupling method; dynamic simulation; shear induced self-diffusion; particle velocity fluctuations.

INTRODUCTION

Understanding the dynamics of suspended solid particles embedded in a viscous carrying fluid is assuming greater importance in industrial applications, driven by both environmental issues and optimization of operating costs in Chemical Engineering. Liquid−solid dispersions may be fluid, paste or solid, depending on the volumetric concentration of solid and the surface interactions of particles. In moderately concentrated suspensions (volumetric concentration up to 20%), a relative motion of the particles is generally always possible and the whole suspension behaves as a fluid with effective properties. Practical applications may be found in water waste treatment, slurry flows and even in biotechnologies. Even paste mixtures may be subject to modification of rheological properties, showing shear-thinning or shear-thickening behaviour depending on the physicochemical treatment that controls particle interactions.

Sheared suspensions are sites for migration and mixing of particles in various viscometer flows. We are concerned only with suspensions of macroscopic particles leading to negligible effect of interparticle forces through surface interactions. Considering a suspension of monodisperse particles embedded in a sheared viscous fluid, the physics of interactions is basically characterized by the following dimensionless parameters: Stokes, Reynolds, Archimedes and Péclet numbers. The Stokes number $St = \rho_\mathrm{p} Ga^2/9\mu$ evaluates the ratio between the time required by the suspended particles to relax after a sudden local fluctuation of the surrounding flow and the fluid time scale G^{-1} (G being the shear rate) and the time required by the suspended particles to relax after a sudden local fluctuation of the surrounding flow (ρ_p and a are respectively the density and the radius of the particles). Particles and

fluid usually have different densities. Then, the Archimedes number ($Ar = ga^3\rho_f(\rho_p - \rho_f)/\mu_f^2$) compares the relative effect of buoyancy and viscous forces. Due to the buoyancy force, particles may settle under gravity with a typical velocity V. The Reynolds ($Re = \rho_f aV/\mu_f$) compares the inertial to viscous effects in the flow, ρ_f and μ_f being the fluid density and viscosity. In the case of small particles, Brownian agitation may contribute to the evolution of the microstructure of the suspension. Hence, the Péclet number ($Pe = 6\pi\mu_f V/k_B T$) compares the convective motion of the particles to their thermal agitation energy $k_B T$. Other non-dimensional parameters may be formed by combination of these numbers. As we neglect surface interactions, the magnitude of attraction and repulsion forces does not need to be compared to inertia or viscous effects.

The dependence of the dimensionless numbers on the particle size and liquid kinematic viscosity in uniformly sheared suspensions ($G = 10\,\text{s}^{-1}$ is a typical shear rate of classical applications) is provided in Figure 1. Horizontal lines correspond to a constant liquid viscosity varying between $10^{-6}\,\text{m}^2\,\text{s}^{-1}$ (water) and $10^{-4}\,\text{m}^2\,\text{s}^{-1}$ (oil). Constant particle radii are marked by vertical dashed lines. Solid lines correspond to dimensionless numbers equal to unity. Brownian motion has to be considered when the suspension properties are located on the left of the line $Pe = 1$ and can be neglected when $Pe \gg 1$. Particle trajectories are weakly influenced by gravity and inertia effects on the left of $Ar/Re = 1$ and $St = 1$, respectively, while the particle behaviour is controlled by buoyancy and inertial effects on the right of these lines. For the line $Re = 1$, suspensions standing on the left are described by Stokes equations, whereas Navier–Stokes equations describe the fluid motion on the right of this line.

In this paper, we aim at investigating numerically the behaviour of non-colloidal liquid–solid sheared suspensions of neutrally buoyant particles in the limit of creeping flow. The suspensions are macroscopically homogeneous and the particle inertia and buoyancy are neglected. Following the non-dimensional analysis (Figure 1), such conditions are fulfilled for a variety of suspensions characterized by particle diameter in the range O (1 μm) suspended in a viscous liquid (kinematic viscosity higher than $10^{-4}\,\text{m}^2\,\text{s}^{-1}$). Designing processes where suspensions have to be fluidized and

transported is often based on the knowledge of the macroscopic behaviour of this complex two-phase flow. Chemical engineers need to model the effective physical parameters that control the response of the system to various flow configurations. Both effective viscosity in the bulk and dispersion coefficient are often evaluated by semi-empirical law. The simulations provide an efficient way to relate the local microstructure of the flow to the global quantities which control the overall behaviour. In order to achieve a clear understanding of the physics of suspension in flow with velocity gradients, we propose to select the fundamental configuration of a pure linear shear flow of monodisperse spherical particles. The flow is unbounded and there are no geometry constraints, such as the presence of walls, to modify the statistic homogeneity of the suspension. In that situation, the statistics are only functions of the volumetric concentration of solid in the bulk.

The velocity gradient in a sheared suspension generates relative motions of particles and therefore hydrodynamic interactions. An analytical investigation of the hydrodynamic interactions between a pair of particles began with the pioneering work of Batchelor and Green (1972). The flow can be split in a far field interaction and a short range velocity perturbation accounting for the lubrication effect. Interactions between three spheres were studied by Wang et al. (1996) using far-field and near-field asymptotic velocity expressions. Lately, Drazer et al. (2004) have investigated the microscopic structure (pair probability distribution function) and macroscopic transport properties of sheared suspensions (translational and rotational velocity fluctuation tensors) from low to high concentration in the case of homogeneous monodisperse suspensions. Although the Stokesian dynamics method they used gave an accurate solution of the Stokes equations, the authors were limited to simulating the simultaneous motion of a few hundred particles because of large time requirement of the numerical approach. They found that a sheared suspension where the particles are initially randomly distributed remains homogeneous in time, but pairs of interacting particles are promoted by the shear, especially when the concentration increases. The fore-aft symmetry of the pair probability distribution function is broken by the effect of non-hydrodynamic repulsive forces when approaching close particles. They highlighted the difference between the statistics of dynamic simulations where the particles driven by the shear flow are free to move when time goes on and the static simulations where the averages are formed over different frozen random particle distributions. In both cases velocity fluctuations are anisotropic and they follow the dilute limit theory estimate based on pairwise interactions up to a 15% volume concentration. However, the fluctuations resulting from dynamic interactions are higher.

In a former work, Drazer et al. (2002) showed that the probability distribution function of the velocity fluctuations have an exponential shape at low concentrations as a signature of long term correlated structures. They appeared to be Gaussian at high concentrations where hydrodynamic screening is achieved by the random multi-body interactions. Lagrangian velocity autocorrelation functions computed by Marchioro and Acrivos (2001) and Drazer et al. (2002) decay with time and have a negative loop located around a characteristic time scale of order $1/G$ (where G is the flow shear rate). This scaling shows that particle trajectories are basically controlled by pair encounters at low concentration. The velocity fluctuations remain correlated for a long time
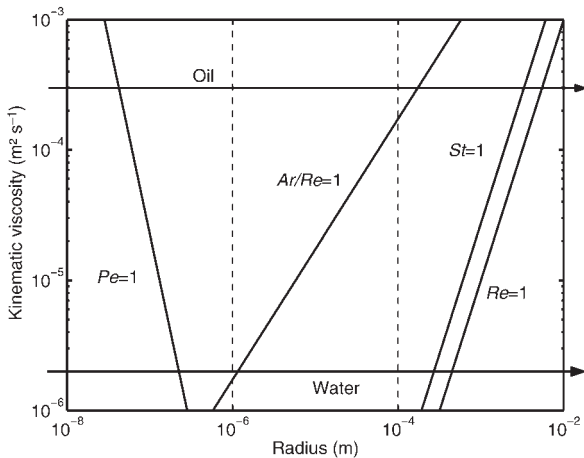

Figure 1. Dependence of the dimensionless numbers on the suspension parameters (particle radius and kinematic viscosity). Each oblique solid line delimits the regions where the dimensionless numbers are respectively lower and higher than unity.

scale (of order $8/G$). A chaotic evolution of the suspension follows the loss of correlation, which is known to lead to the shear induced diffusion even at high Péclet number. Diffusion in such conditions has been studied in many works, starting from the reference experimental work of Leighton and Acrivos (1986), to analytical calculations of Wang *et al.* (1996) based on three particle interactions, to new experimental techniques developed by Breedveld *et al.* (1998, 2001, 2002) and numerical simulations of Marchioro and Acrivos (2001), Drazer *et al.* (2002), Sierou and Brady (2004). Self-diffusion coefficients reported in these works are anisotropic and strongly increasing with the suspension concentration. Results obtained from different works achieve only a qualitative agreement.

In this paper, we propose to use the force coupling method as a numerical model to solve the Stokes equations accounting for the velocity perturbations induced by hydrodynamic interactions of particles. This is a fully coupled numerical model, simulating dynamic interactions between thousands of particles under the approximation of Stokes flow. First, we briefly describe the numerical model which has been validated in various configurations of Stokes flows. We propose some quantitative tests which control the accuracy of the model in the present configuration of a linear shear flow. In the following sections, macroscopic quantities are investigated by computing the velocity fluctuations, their probability density function and Lagrangian autocorrelation functions. Self-diffusion coefficients are then calculated. Aiming to look at the suspension from a microscopic level, we computed statistics highlighting the preferential orientation of interacting pair of particles. We compare our results on statistical quantities to the work of Drazer *et al.* (2002, 2004) which used the Stokesian dynamics to compute interactions in the same context of suspension dynamics. Finally, we conclude on the ability of the force coupling method for simulating the flow of suspensions and propose perspectives to this study.

THE FORCE COUPLING METHOD

The complexity of dispersed two-phase flows is related to the numerous length scales that have to be resolved simultaneously. In the case of Stokes flows, the velocity disturbance induced by a single particle falls off very slowly and then multi-body hydrodynamic interactions control the evolution of the suspension. We propose to use a numerical model, which is able to couple simultaneously the solution of fluid flow equations and the Lagrangian tracking of the particles. The force coupling method (FCM) is based on a low order multipole expansion of the velocity disturbance induced by the presence of particles. The equations of the fluid motion are solved directly and the forcing term is modeled by a spatial source of momentum added to the Stokes equations. The accuracy of the model increases as we add higher order terms in the multipole expansion, but solving the equations becomes more time consuming.

Model Equations

Details on the theoretical background of the FCM can be found in the paper of Maxey and Patel (2001). We describe briefly the basic equations. We consider that the fluid is incompressible [equation (1)], has a constant viscosity μ,

and we neglect its inertia. The fluid velocity field $\mathbf{u}(\mathbf{x}, t)$ and the pressure $p(\mathbf{x}, t)$ are solutions of the Stokes equations [equation (2)].

$$\nabla \cdot \mathbf{u} = 0 \tag{1}$$

$$0 = -\nabla p + \mu \nabla^2 \mathbf{u} + \mathbf{f}(\mathbf{x}, t) \tag{2}$$

The forcing term on the right hand side of equation (2) is a spatial distribution of momentum which is induced by the presence of the moving particles. This term is spatially and temporally evolving while the particles are freely moving under hydrodynamic interactions. Its expression is based on theoretical analysis of low Reynolds number flows. We consider only two terms [see equation (3)] of the multipole expansion of finite source terms, namely the force monopole (Stokeslet) and the force dipole.

$$f_i(\mathbf{x}, t) = \sum_{n=1}^{N_B} F_i^{(n)} \Delta[\mathbf{x} - \mathbf{Y}^{(n)}(t)]$$
$$+ G_{ij}^{(n)} \frac{\partial}{\partial x_j} \Delta'[\mathbf{x} - \mathbf{Y}^{(n)}(t)] \tag{3}$$

The N_B particles are centered at locations $\mathbf{Y}^{(n)}(t)$ and the source terms are spread out on the flow field using finite size envelopes [equation (4)]. The width of the Gaussian envelopes [σ for $\Delta(\mathbf{x})$ and σ' for $\Delta'(\mathbf{x})$, respectively] are related to the particle radius a by analytic expressions with

$$\Delta(\mathbf{x}) = (2\pi\sigma^2)^{-3/2} e^{(-|\mathbf{x}|^2/2\sigma^2)} \tag{4}$$

The magnitude of the interaction force $\mathbf{F}^{(n)}$ is directly related to the force acting by the fluid on the considered particle. It is a combination of buoyancy, inertia effect and an external force $\mathbf{F}_{\text{ext.}}$ [equation (5)], and it cancels for non-buoyant particles driven by the shear flow at low Stokes number.

$$\mathbf{F}^{(n)} = (m_P - m_F)\left(\mathbf{g} - \frac{d\mathbf{V}^{(n)}}{dt}\right) + \mathbf{F}_{\text{ext}}^{(n)} \tag{5}$$

$G_{ij}^{(n)}$ is a tensor which can be split into symmetric and anti-symmetric parts ($G_{ij}^{(n)} = S_{ij}^{(n)} + A_{ij}^{(n)}$). The symmetric part (namely, the Stresslet) contributes to enforce a solid body rotation within the fluid occupied by the particle. The iterative scheme on a steepest descent scheme that was used to enforce a zero strain rate within the particle volume is described in details in the work of Dance and Maxey (2003). The anti-symmetric part $A_{ij}^{(n)}$ is related to the external torque $T^{(n)}$ acting on the particle n [equation (6)] where $A_{ij}^{(n)} = \frac{1}{2}\varepsilon_{ijk}T^{(n)}$

$$\mathbf{T}^{(n)} = -(I_P - I_F)\left(\frac{d\mathbf{\Omega}^{(n)}}{dt}\right) + \mathbf{T}_{\text{ext}}^{(n)} \tag{6}$$

m_P (resp. m_F) is the mass of the particle (resp. fluid) volume and I_P (resp. I_F) is the particle (resp. fuid) rotational inertia. Throughout the paper, both the translational and rotational inertia of particles will be neglected. Neglecting particle inertia restricts the scope of our study to the important class of problems related to solid−liquid suspensions with moderately density ratio. The ratios a/σ and a/σ' are set as to match respectively Stokes drag for an isolated sphere (radius a)

and to ensure an average zero rate of strain [equation (7)] within the volume occupied by the particle.

$$S_{ij}^{(n)} = \frac{1}{2}\int\left(\frac{\partial u_i}{\partial x_j} + \frac{\partial u_j}{\partial x_i}\right)\Delta'\left(\mathbf{x} - \mathbf{Y}^{(n)}(t)\right)d^3x = 0 \qquad (7)$$

These requirements are fulfilled exactly in the limit of Stokes approximation while a/σ and a/σ' are set analytically for a Gaussian shaped envelope: $a/\sigma = \sqrt{\pi}$ and $a/\sigma' = (6\sqrt{\pi})^{1/3}$ (see details in Maxey and Patel, 2001; Lomholt and Maxey, 2003). In a sheared suspension, the monopole is negligible for non-buoyant spheres, and the Stresslet will be the major contribution.

Particles move freely in a Lagrangian framework as their trajectory equations are solved simultaneously. Particle velocities and rotation rates are obtained with a spatial filtering of the flow velocity field based on the spherical Gaussian envelop [equations (8) and (9)].

$$\mathbf{V}^{(n)}(t) = \int \mathbf{u}(x, t)\Delta\left[\mathbf{x} - \mathbf{Y}^{(n)}(t)\right]d^3\mathbf{x} \qquad (8)$$

$$\mathbf{\Omega}^{(n)}(t) = \int \nabla \times \mathbf{u}(x, t)\Delta'\left[\mathbf{x} - \mathbf{Y}^{(n)}(t)\right]d^3\mathbf{x} \qquad (9)$$

Then, the trajectory of each particle is computed by integrating equation (10).

$$\frac{d\mathbf{Y}^{(n)}}{dt} = \mathbf{V}^{(n)}(t) \qquad (10)$$

More details on the theoretical background and an extensive validation of the method are available in Maxey and Patel (2001), Lomholt *et al.* (2002), Lomholt and Maxey (2003).

Validation Tests and Accuracy

The multipole decomposition truncated to the first order (force monopole) is not sufficient when near field interactions have to be accounted for. Therefore, the flow resolution may be improved by incrementing the order of the multipole decomposition. The accuracy of the FCM is increased by adding the force dipole in the source term. An iterative scheme is used to enforce a zero rate of strain within the volume occupied by the particles.

Neutrally buoyant particles moving in a shear flow experience only the symmetric dipole forcing. When a single particle is seeded in a linear shear flow, it is driven by the mean flow velocity (i.e., $V_1 = Gx_2$). The presence of the solid particle which is freely rotating induces a velocity perturbation in the fluid flow. The perturbation velocity field has a fore-aft symmetry. It is strained along the compression axis of the mean flow (in the shear plane). The velocity perturbation related to an isolated single particle in an unbounded fluid was calculated analytically in the paper of Batchelor and Green (1972). Comparing the velocity profiles with our numerical simulations, we observed that the far-field approximation is perfectly reproduced and only slight differences appear close to the particle surface. The agreement is within few percent when the distance to the centre is larger than 1.25 particle radius. Obviously the discrepancy is caused by the representation of particles by distributed momentum source terms without an actual separation between the fluid and the solid body rotation. The presence

of the particles is enforced by the constraint [equation (7)] on the local strain rate of the velocity perturbation.

The same authors have also determined analytical expressions for the relative velocity [equation (11)] and rotation rate [equation (12)] for an interacting pair of particles in a shear flow. The velocities are expressed in terms of three non dimensional scalar functions (A, B and C) which depend only on the particle non-dimensional separation distance r/a.

$$\mathbf{V}(r) = -G\begin{cases} r_2\left(B/2 + r_1^2/r^2(A - B)\right) \\ r_1\left(B/2 + r_2^2/r^2(A - B)\right) \\ r_1r_2r_3/r^2(A - B) \end{cases} \qquad (11)$$

$$\mathbf{\Omega}(r) = -\frac{CG}{2}\begin{cases} r_1r_3/r^2 \\ -r_2r_3/r^2 \\ (r_2^2 - r_1^2)/r^2 \end{cases} \qquad (12)$$

$\mathbf{r} = (r_1, r_2, r_3)$ is the separation distance between the two particle centres and G is the shear rate of the flow. The direction 1 is for the mean flow direction, 2 is for the direction of shear and 3 is for the vorticity direction normal to the plane of shear. The evolutions of A, B and C are shown in Figure 2 for two equal spheres. The numerical simulations are in good agreement with the analytical expressions when the gap between the two particles is larger than 25% of the particle radius. For extremely close particles, the lubrication effects should be accounted for with more accuracy (short-range hydrodynamic interactions). Based on a parameterization developed by Dance and Maxey (2003), we showed in a former work (Abbas *et al.*, 2006) that when adding the lubrication forces to the FCM in a pair-wise additive manner, the calculation of the interaction between close particles is significantly improved. The accuracy of the numerical approach limits the scope of our study to moderately concentrated suspensions.
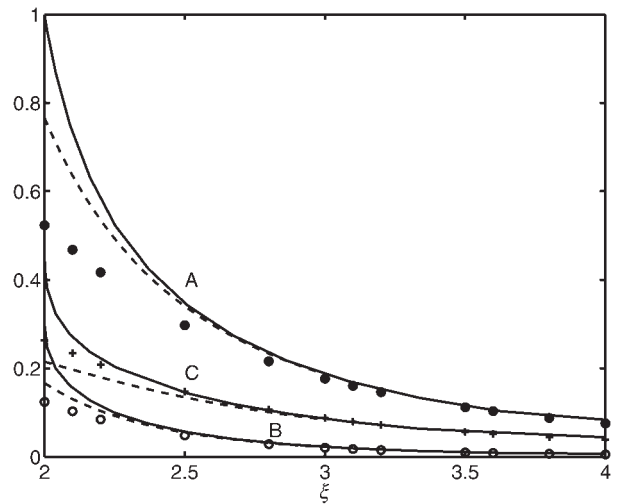

Figure 2. The dependence on the separation distance between particle centers ($\xi = r/a$) of the hydrodynamic parameters. Solid lines: analytic solution; dashed lines: far-field approximation; symbols are FCM results. Filled circles: A; empty circles: B; plus: C.

Repulsion Barrier

The FCM is only an approximate model since fluid occupies the whole domain and no-slip boundary conditions on the particle surface are not strictly imposed. In Stokes flow, actual contact between particles is very limited because lubrication effects drastically slow down the approach of particles. A repulsive force $\mathbf{F_b}$ is added to the monopole coupling term when the distance between the particle centres r is less than a prescribed cut-off separation distance R_{ref}. This repulsive barrier [equation (13)] is used to fix a numerical inaccuracy of the model by preventing particles from overlapping (Figure 3).

$$\mathbf{F_b} = -\frac{F_{ref}}{2a}\left[\frac{R_{ref}^2 - r^2}{R_{ref}^2 - 4a^2}\right]^2 \mathbf{r} \qquad (13)$$

Once it is switched on, the repulsion barrier drives particles rolling on the surface of each other preventing them from overlapping (Figure 3). Different tests were carried out to verify that the trajectories are only slightly modified by large variation of the cut-off distance R_{ref} and the force scale F_{ref}. When the cut-off distance is considerably reduced ($R_{ref} = 2.2a$ to $R_{ref} = 2.02a$), the minimum gap between the particle surfaces varied but no significant difference was observed on the particle trajectories. The time step has to be reduced (in a one-fifth ratio) so that the short range interactions are well resolved. All the simulations analysed in this paper were done with $R_{ref} = 2.2a$ leading to a minimum gap smaller than one percent of the particle radius.

Although this force is used for preventing particle overlap, it could be interpreted in terms of physical considerations. Even when particles in solid–liquid suspensions are not charged they generally experience a short range interparticle force due to the double layer electric repulsion (DLVO-type) when the gap is shorter than $10^{-2}a$. The suspensions that we study may be considered as stabilized suspensions while a strong repulsive force prevent the formation of permanent cluster of particles. Short range attraction forces, such as the Van der Waals potential, are screened by hydrodynamic lubrication force and the repulsive barrier. The physical analog of our simulations would be the case where electrostatic repulsive forces (proportional to the fluid permittivity $\varepsilon_r\varepsilon_0$ and to the square of particle surface potential ψ^2) are overcoming the Van der Waals attraction force (related to the Hamaker constant Λ).

A practical example of suspension that fits the assumptions of our simulations may be composed of polystyrene latex spheres of 2 μm radius in a 50% glycerol-in-water mixture containing 10^{-3} mol l^{-1} KCl, undergoing a flow shear rate of 1 s^{-1}. A DLVO-type interaction is characterized by the particle surface potential $\psi \approx 4$ mV and a Debye length $\kappa^{-1} = 88$ Å giving $\varepsilon_r\varepsilon_0 \approx 5.9 \times 10^{-10}$ C^2 Jm^{-1} (Brady and Bossis, 1985). The dynamic fluid viscosity and density are respectively about 4×10^{-3} Pa s and 1.126 kg m^{-3}. For such a suspension, the non-dimensional numbers $2\pi\varepsilon_r\varepsilon_0\psi^2a/\Lambda \approx 15$ and $2\pi\varepsilon_r\varepsilon_0\psi^2a/\mu_f Ga^3 \approx 3.5$ confirm that the electrostatic repulsive potential overcomes the attraction and shear-induced energies. We calculated the Archimedes/Reynolds, Stokes, Reynolds and Péclet numbers and obtained respectively 8.5×10^{-3}, 2.4×10^{-7}, 10^{-6} and 160.

At these scales, the effect of roughness and residual Brownian motion may be an issue because the particle radius is $O\,(1\,\mu m)$. These phenomena would also behave as a repulsive contribution and they can be simply modelled by a repulsive force, although the precise magnitude and form are unknown. When particles are far enough $r > R_{ref}$, the repulsion barrier [equation (13)] is switched off and the dipole terms only control the motion of the particles. While the gravity and the particle inertia are neglected, the Stokeslet is always zero unless when the interaction forces $F_{ext}^{(n)}$ is switched on: $r < R_{ref}$. This rough treatment of the near-field hydrodynamics of particles near contact may restrict the accuracy of the model. We investigate only low to moderately concentrated suspensions (volumetric concentration lower than 20%). Careful tests in similar conditions have shown that the impact of this repulsive force on the overall dynamics of the suspension is weak (Dance *et al.*, 2004; Da Cunha and Hinch, 1996).

Information on the Simulations

Simulations are performed in a cubic domain whose width L is kept constant and equal to 2π. Various volumetric concentrations of the suspension are obtained by changing the particle number in the domain, typically 3200 particles for a 12% concentration. The particle diameter is kept constant for different concentrations, and extends over six grid nodes. Stokes equations are solved with a spectral Fourier algorithm and particle tracking is achieved through a fourth order Adams-Bashforth scheme. In order to preserve the homogeneity of the suspension flowing under a linear shear, we impose periodic boundary conditions in the three directions. Most simulations have been carried out with $L/a = 48$, with 128^3 mesh grids so that the influence of the periodic images of any particle in the domain is considerably reduced. The numerical scheme used for the solution of the Stokes equations takes advantage of the periodic boundary conditions by using Fast Fourier Transforms. We used a domain decomposition algorithm to achieve scalable performance on parallel supercomputers. Typical runs need four processors and statistics are converged over a 30-h computation.
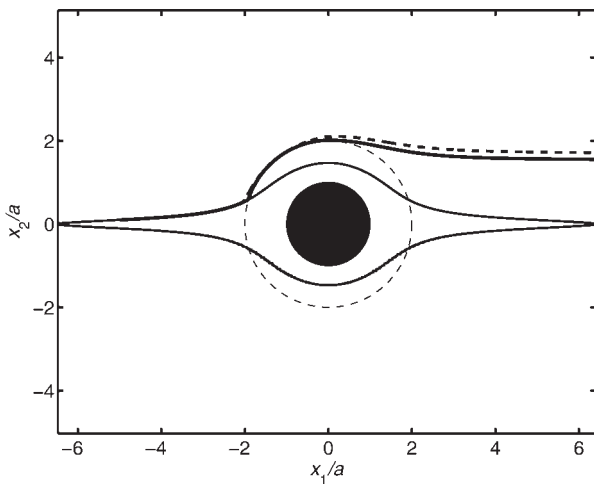

Figure 3. Relative two particle trajectories in a shear flow for different values of the repulsion barrier parameters. Filled circle: surface of the reference particle. Dashed circle: overlapping limit. Thin solid line: $F_{ref} = 0$. Thick solid line: $F_{ref} = 0.3$, $R_{ref} = 1.02$, $dt = 2 \times 10^{-3}$— dashed line: $F_{ref} = 0.3$, $R_{ref} = 1.2$, $dt = 10^{-2}$

The Stokes equations are linear, so we only solve the flow perturbation induced by the presence of the particles (Stresslet contributions) and superimpose the linear shear flow $u_1 = Gx_2$ (G is the shear rate) on the particle motions. Statistical information can be obtained by means of two distinct procedures: a 'static' one where the averages are formed on independent sets of random seeding of the particles and a 'dynamic' one where the averages are computed while the suspension evolves in time. The static procedure may seem unusual. Stokes equations are not intrinsically time dependent (no inertia effect) because the velocity field depends only on the relative positions of the particles. Then, in a 'static' simulation, particles are randomly seeded with non-overlapping positions in the sheared suspension. For each independent configuration, the computation of hydrodynamic interactions provides the flow velocity distribution and consequently the particle velocities [see equations (1), (2), (8) and (9)]. These simulations can be regarded as a model of the perfectly random microstructure.

The 'dynamic' way to form averages accounts for the evolution in time of the suspension. In that case, particles are initially seeded at random positions. Then, trajectories are computed as a sequence of fully coupled interactions between the fluid and the particles [equations (1), (2), (8), (9) and equation (10) additionally]. The trajectories are integrated with a constant time step $5 \times 10^{-3} \, G^{-1}$. This corresponds to a decrement of $a/100$ of the separation distance between two approaching particles. When a particle exits the simulation domain from the bottom (resp. upper) boundary, it appears on the opposite side, and its velocity must be adjusted by adding (resp. substracting) the local flow velocity GL. This is equivalent to applying the shear in a dynamic way by means of the Lees-Edwards boundary conditions (Allen and Tildesley, 1987). Ensemble averages are formed over all the particles as time goes on. The typical length, time and velocity scales are a, G^{-1} and aG, where a is the particle radius. Typically, we simulate the suspension flow during a dimensionless time Gt proportional to $100 \, \phi^{-1/3}$ (ϕ is the volumetric suspension concentration). During this time, a particle is expected to experience enough interactions with other particles to achieve its steady statistical regime. It has been clearly pointed out that the determination of self-diffusion coefficients needs very long time series for reaching the diffusive behaviour (Sierou and Brady, 2004) of the suspension and this point will be carefully checked later.

In this paper, velocity fluctuations and microstructure organizations were calculated and compared for both static and dynamic simulations. However, statistical quantities like velocity autocorrelations and shear-induced diffusion are obviously calculated only in dynamic suspensions after a long time of shearing. We checked that the results do not depend on the initial random seeding when a 128^3 grid is used. Simulations performed with smaller resolution (and consequently fewer particles) need to be averaged on distinct initial seeding. This was a shortcoming of previous studies using Stokesian dynamics which is more time consuming.

VELOCITY FLUCTUATIONS AND MICROSTRUCTURE OF THE SUSPENSION

Velocity Fluctuations

Although the suspension is globally homogeneous, particles are not moving with the same instantaneous velocities.

At a scale related to a few particle radii, velocity perturbations are not uniform in the suspension as they strongly depend on the relative particle positions. If isolated, or far from each other, the particles would be driven by the local unperturbed velocity of the flow. However, in a sheared suspension the particle velocities are subject to fluctuations induced by their interaction with the fluid and with each other. The determination of the exact perturbations due to hydrodynamic interactions between a pair of particles has been done analytically by Batchelor and Green (1972). But when more than two particles are involved in the flow, the equations become very complicated and no analytical solution exists (only far-field approximations can be achieved) (Wang et al., 1996). Based on the work of Batchelor and Green (1972) and on the explicit relations given by Da Cunha and Hinch (1996), Drazer et al. (2004) have predicted theoretically the evolution of the translational and rotational fluctuation tensors [equations (14) and (15)] in the dilute regime. They used two approximations for the microstructure of the suspension. In the dilute limit, the purely random pair probability density function (derived from 'static' simulations) models relative positions of the particles that are not correlated. On the other hand, the pair probability density function derived by Batchelor and Green (1972) is accounting for hydrodynamic interactions in a shear flow ('dynamic' simulations). Following symmetry arguments in a dilute suspension, the diagonal terms T_{11} and T_{22} of the dimensionless translational fluctuation tensors (resp. w_{11} and w_{22} for rotation) are equal, and different from T_{33} (resp. w_{33}). The off-diagonal terms are strictly zero when the fore-aft symmetry is preserved (purely random static suspension).

$$(Ga)^2 T_{ij} = <v_i v_j> - <v_i><v_j> \tag{14}$$

$$G^2 w_{ij} = <\Gamma_i \Gamma_j> - <\Gamma_i><\Gamma_j> \tag{15}$$

In equations (14) and (15), $\mathbf{v}$ and $\mathbf{\Gamma}$ are, respectively, the translational and rotational particle velocity perturbation (the difference between the instantaneous velocity of the particle $\mathbf{V}$ (resp. $\mathbf{\Omega}$) and the local unperturbed fluid velocity $u_1 = Gx_2$ (resp. $w_3 = (\nabla \times \mathbf{u}) \cdot \mathbf{e}_3$). $<>$ stands for averages in time and over all the particles. We verified that $<v_i>$ and $<\Gamma_i>$ are vanishingly small when averages are formed over long time series $[<v_i><v_j>/<v_i v_j> = O(10^{-5})]$.

We first simulate the evolution of the fluctuation tensors with the concentration in a static configuration. Averages are formed over more than 100 uncorrelated random seeding of the particles. In Figure 4(c) and (d), translational and rotational velocity fluctuations are compared to the theoretical prediction of Drazer et al. (2004), based on pairwise interactions for a purely random pair probability function. The fluctuations scale linearly with the concentration (especially for low suspension concentration) and they are highly anisotropic. The fluctuations in the flow and shear directions (T_{11} and T_{22}, resp. w_{11} and w_{22}) are equal. The translational (resp. rotational) fluctuation in the spanwise direction T_{33} (resp. w_{33}) is nearly four times lower (resp. larger) than the fluctuations in the other directions. The highest velocity fluctuations take place in the plane of shear. All these results are in good agreement with the theory.

The behaviour of all the diagonal terms of the velocity fluctuations is similar in both dynamic and static simulations when the concentration increases [Figure 4(a) and (b)].
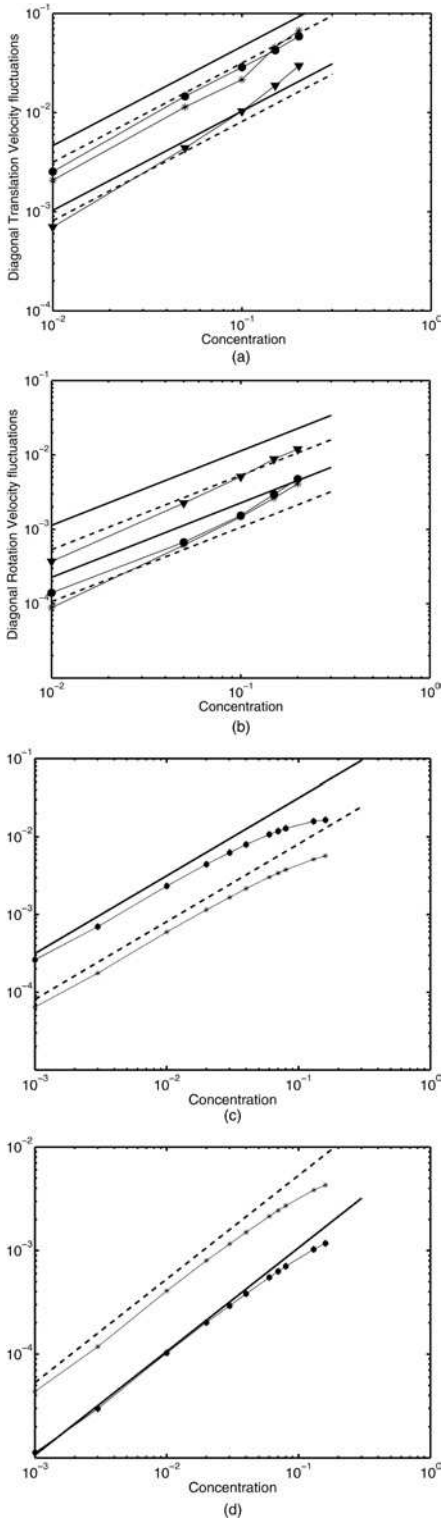
Figure 4. Diagonal terms of the (a) translational and (b) rotational velocity fluctuation tensors versus concentration with dynamic simulation conditions. Stars: T_{11} and w_{11}—filled circles: T_{22} and w_{22}—filled triangles: T_{33} and w_{33}. Solid lines: dilute limit theory based on the pair probability function of Batchelor and Green (1972). Dashed lines: dilute limit theory assuming a random distribution in a static simulation. Diagonal terms of the (c) translational and (d) rotational velocity fluctuation tensors versus concentration with static simulation conditions. Superimposed filled circles and diamonds: (c) T_{11} and T_{22}, (d) w_{11} and w_{22}—Stars: (c) T_{33} and (d) w_{33}. Solid and dashed lines: dilute limit theory assuming a random distribution in a static simulation.

However, velocity fluctuations resulting from shear-induced particle interactions are nearly two times larger than in the static simulations. A linear scaling was expected to occur up to moderately concentrated suspension (20%) as the velocity perturbation induced by the Stresslet contribution decays like $1/r^2$. Fluctuations for extremely low volume fractions in the dynamic simulations were not calculated since the corresponding computations need a very long time to converge.

While the theoretical prediction assumes fore-aft symmetry of the relative trajectory of a particle pair, zero off-diagonal terms are expected. Figures 5(a) and (b) confirm the theory for all off-diagonal terms except T_{12} and w_{12} in the case of dynamic simulations. According to the work of Drazer *et al.* (2004) we found that T_{12} (resp. w_{12}) is negative (resp. positive) and its magnitude increases with the concentration. As off-diagonal terms are not zero, it suggests that a symmetry breaking occurs following the particle interactions. This is induced by the repulsive non-hydrodynamic force but also due to multi-body interactions. The symmetry breaking is clear in Figure 6 where the particle positions close to contact (particle centers closer than $2.5a$ are recorded on the plot)
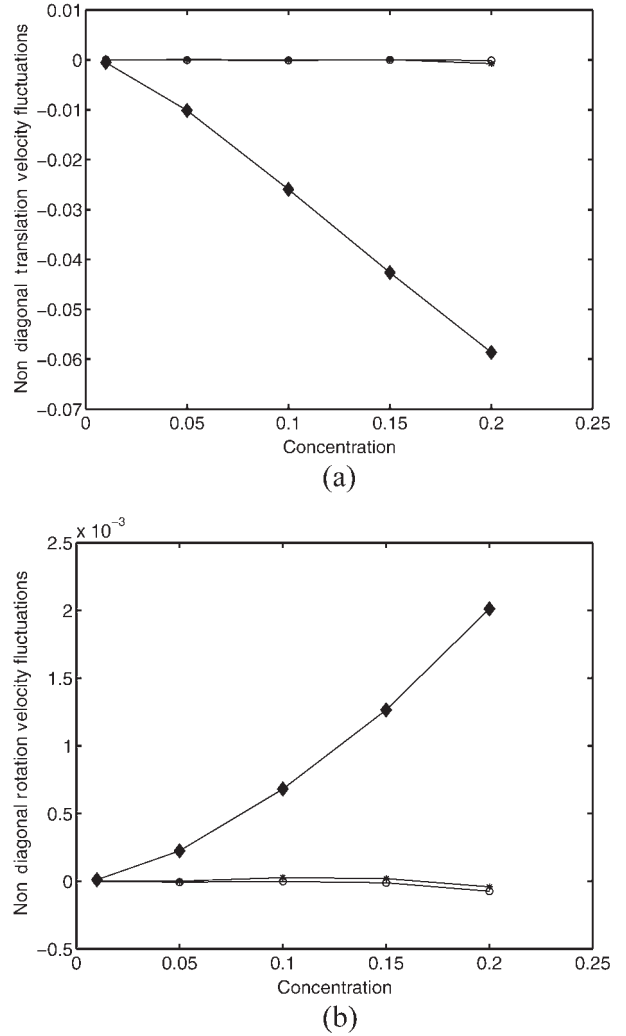

Figure 5. Off-diagonal terms of the (a) translational and (b) rotational velocity fluctuation tensors versus concentration with dynamic simulation conditions. Filled diamonds: T_{12} and w_{12}.
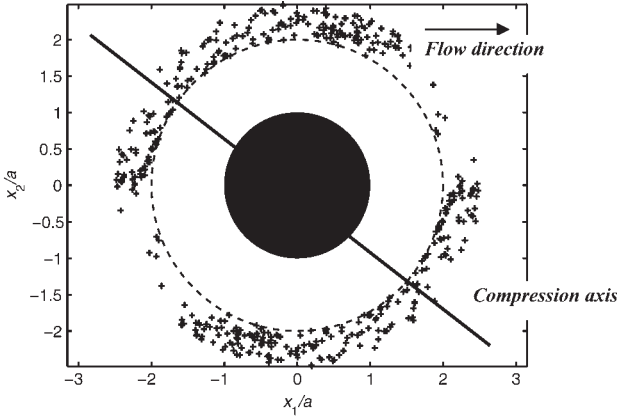
Figure 6. Relative positions of particle pairs in a shear flow. Filled circle: reference particle. Dashed circle: limit of the overlapping region (where $r < 2a$). $+$: Location of particle centres close to contact relatively to the reference particle ($r < 2.5a$). The figure is populated with several independent time frames. The compression axis is materialized by a solid line.

appear to be highly anisotropic. The main contribution of the shear flow is to enhance interactions along the compression axis. Then, the repulsion barrier leads to depletion in the receding side of the reference particle. Such a symmetry breaking enhances the occurrence of negative (resp. positive) cross-products v_1v_2 (resp. $\Gamma_1\Gamma_2$) of the velocity perturbations [see equations (11) and (12)].

Pair Probability Density Function

Contrary to purely random seeding where particle pairs do not have any angular preferential orientation ($T_{12} = 0$, $w_{12} = 0$) it is clear from Figure 6 that an anisotropic angular structure is developing in time in a sheared suspension ($T_{12} < 0$, $w_{12} > 0$). A large number of particle pairs are oriented along the compression axis of the flow compared to the depletion of the receding side. Hydrodynamic interactions increase when the particles approach from each other driven by the flow velocity gradient, and particle pairs are found to remain in close vicinity for an extended time before separation occurs. The depletion of the particle pairs on the receding side is enhanced by the non-hydrodynamic repulsive force even if the lubrication force acting when particles are close to contact should restore the symmetry. Such weak irreversible effects, which are present at a microscopic scale have a measurable impact on the macroscopic structure of the suspension and consequently on the effective quantities such as velocity fluctuations T_{12} and shear-induced self-diffusion as will be discussed later (Zarraga and Leighton, 2001). The radial and angular pair probability density function is not proposed in this paper since it needs very long simulation time to converge. However, it is interesting to quantify the microscopic structure organization, at least by calculating the radial dependence of the pair probability density function. It is a quantitative measure of the probability of finding a particle at a separation distance r.

Based on the analytic expressions of the relative velocity of particle pairs in a Stokes shear flow, Batchelor and Green (1972) have theoretically calculated the particle trajectories and the pair probability density function. They showed that

closed trajectories exist leading to a divergent evolution of $g(r)$ at short separation distances. But actually, the non-hydrodynamic interparticle interactions such as surface roughness, repulsive forces or even hydrodynamic interactions between more than two particles, generate a transfer of particles across the streamlines which cancels the probability of finding closed trajectories. Therefore the pair probability function always converges (Brady and Bossis, 1985).

We determined the evolution of the pair probability density function with only the radial separation distance r of particle pairs [equation (16)]. We computed, for each particle, the number $n_i(r)$ of particles that can be found in an elementary volume $dV(r)$ at a separation distance r.

$$g(r) = \frac{4\pi a^3/3}{N\phi dV(r)} \sum_{1}^{N} n_i(r) \qquad (16)$$

As we have shown in Figure 6, the pair probability function is not isotropic and $g(r)$ is integrated over all angular orientations. It is null for separation distance between particle centers corresponding to contact [$g(r < 2a) = 0$] since there is no particle overlapping. The probability function $g(r)$ is normalized using $\int_0^\infty g(r)dr = 1$.

$g(r)$ was computed using both static and dynamic simulations, and for different suspension concentrations. Figures 7(a) and (b) show that the pair probability functions have qualitatively the same behaviour in both cases. The probability of finding particles near contact is maximum leading to a peak value at a separation distance $r/2a = 1$. The peak value increases with the volume fraction ϕ of the suspension. In the static simulations, $g(r)$ results only from the random seeding of particles and the peak denotes only correlations owing to the excluded volume effect. It is clear that close particle pairs have a higher probability to occur when the particles in the suspension are driven by the shear flow. Similar results have been reported for Brownian (Morris and Katyal, 2002) and non Brownian (Brady and Bossis, 1985; Sierou and Brady, 2002; Drazer *et al.*, 2004) suspensions under shear flow.

Probability Distribution Function of Velocity Fluctuations

Normalized probability density functions of the translational velocity fluctuations in the shear direction are shown in Figure 8(a) for four different volume fractions. We obtained basically the same plots in other directions. The first observation is that for weak velocity fluctuations, all the probability density functions have a Gaussian shape, but for higher magnitude of velocity fluctuations the shape gradually changes as the concentration increases. Intense velocity fluctuations are more probable than the Gaussian estimate. For example, in Figure 8(b) (5% concentration), a best fit of the pdf is composed of a Gaussian behaviour for weak velocity fluctuations $|v/s| < 1$ (where s is the standard deviation of the velocity fluctuations) and an exponential tail for intense fluctuations. Such a behaviour is related to the presence of persistent small-scale structures, due presumably to the long-lasting short-range hydrodynamic interactions of pairs of particles at low volume fraction (Drazer *et al.*, 2002). Whereas, when the concentration is increased, the probability density function has a more pronounced Gaussian shape. At large concentrations, the mean separation distance between the
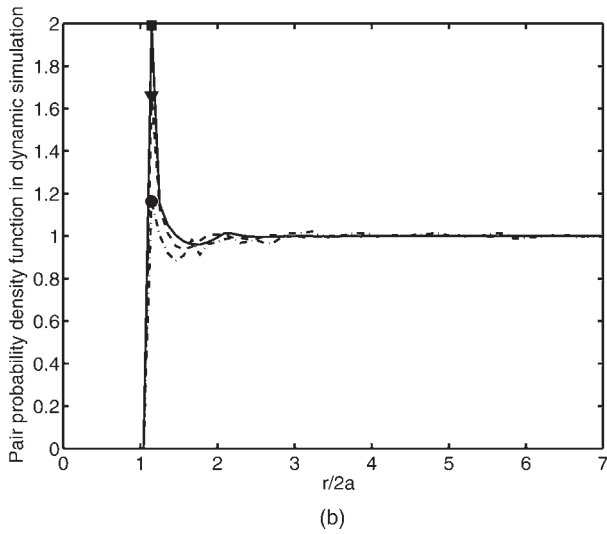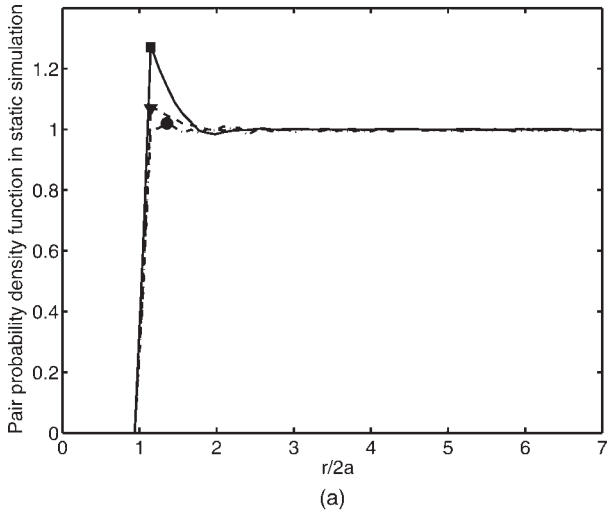
Figure 7. Pair probability density function $g(r)$ calculated in the case of (a) static simulations and (b) dynamic simulations. Symbols •, ▼ and ■ correspond respectively to the peak values of 1, 5 and 15% concentration cases.
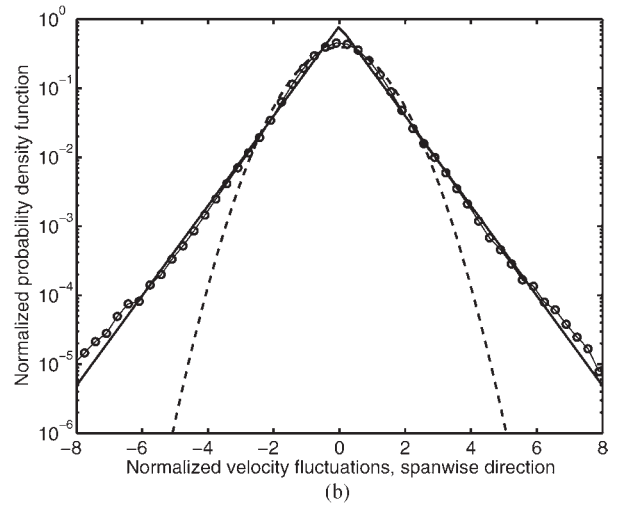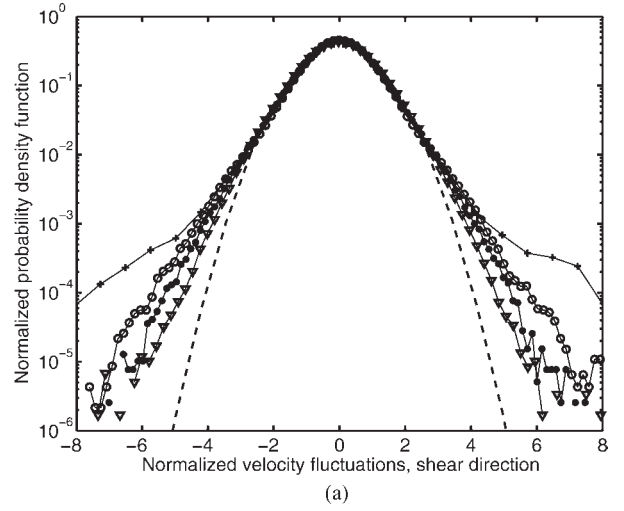
Figure 8. Normalized PDF of particle velocity fluctuations in the (a) shear and (b) spanwise directions. Dashed line: Gaussian distribution function. (a) Plus: $\phi = 1\%$—Circles: $\phi = 5\%$—Stars: $\phi = 10\%$—Triangles: $\phi = 20\%$. (b) Circles: $\phi = 5\%$. Solid line: best fit by a stretched exponential $\text{PDF}(v/s) \approx 2/\sqrt{2\pi} \exp(-1.5|v/s|)$.

particles is reduced leading to multiple many-body interactions with a weaker overall correlation. Similar changes in flow statistics have been observed in a turbulent flow (Verzicco and Camussi, 2001). For low Reynolds numbers the distribution of vorticity fluctuations is almost Gaussian, associated with weakly correlated fluid motions. Whereas when the Reynolds number increases, coherent small scale vorticity structures develop leading to stretched exponential tails. Such behaviour is a common feature of many complex physical systems [in fluidized beds for example, velocity fluctuation distribution varies from Gaussian to exponential as the particle concentration increases (Rouyer *et al.*, 1999)].

VELOCITY AUTOCORRELATION AND SELF-DIFFUSION

Lagrangian Velocity Autocorrelation

Multiple interactions of particles in the flow lead to a chaotic motion in the suspension. Although the Stokes

equations are linear and deterministic, many-body hydrodynamic interactions and repulsion barrier effects force the particles to move across streamlines. The system is extremely sensitive to the initial conditions and even an extremely weak perturbation introduced in the calculation induces a complete loss of memory of the initial state. Such a response is typically related to a diffusive behaviour of the suspension at long times. Figure 9 shows an example of the impact of cumulated numerical errors on the temporal evolution of velocity fluctuations for an 18% suspension concentration. Initial particle positions are identical for the two runs with only a very weak perturbation of order 10^{-15}. The temporal evolutions of T_{22} are superimposed for non-dimensional times lower than 100. Afterwards, the two evolutions have distinct instantaneous evolutions although statistics (mean and standard deviation) are preserved.

The time required to get uncorrelated velocity fluctuations along the particle trajectories is extracted from the normalized Lagrangian velocity autocorrelation function $R_{ii}(t)$
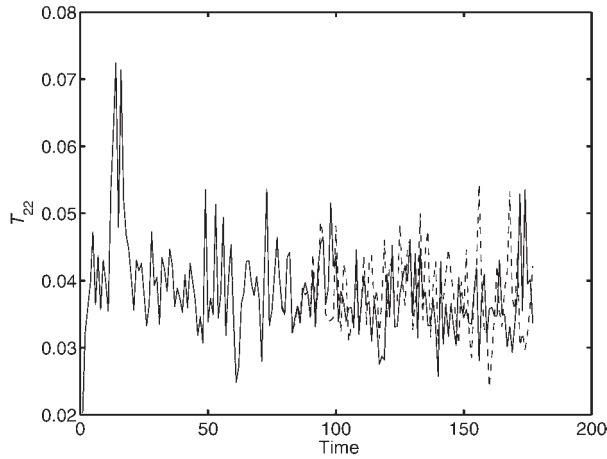
Figure 9. Temporal evolution of the velocity fluctuation in the shear direction T_{22} (18% concentration). Solid and dashed lines show T_{22} obtained during simulations with the same initial conditions and a weak noise (magnitude 10^{-15}).

[equation (17)] computed along the two transverse directions (shear and spanwise direction).

$$R_{ii}(t) = \frac{\langle v_i(\tau)v_i(\tau+t)\rangle}{T_{ii}} \qquad (17)$$

The product $v_i(\tau)v_i(\tau+t)$ is averaged over all the particles for the different starting times τ. In Figure 10 the velocity autocorrelation functions are plot for different suspension concentrations up to 20%. We can observe that in all cases the velocity fluctuation autocorrelations have a negative region around a typical time Tc_1 of order $1/G$ suggesting that pairwise interaction is the major contribution to anti-correlated motions. A two particle encounter has a life time of $1/G$. The negative region is more pronounced at low concentration but is still prominent at moderate concentration in agreement with Marchioro and Acrivos (2001). Another important characteristic time scale Tc_2 is the time required to reach uncorrelated fluctuations. Fully uncorrelated motions are
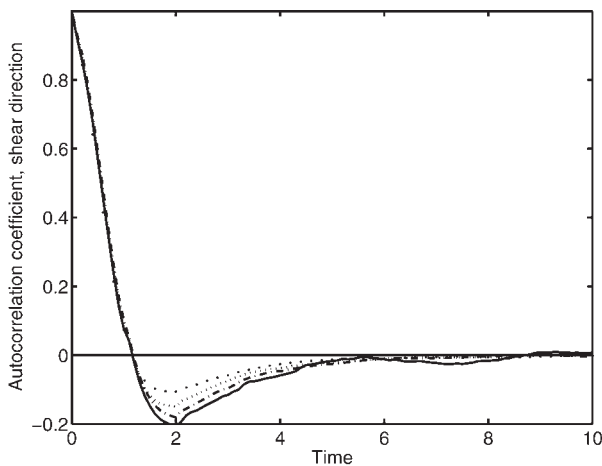

Figure 10. Lagrangian velocity autocorrelation function in the shear direction for different suspension concentrations. —— $\phi = 1\%$, ----·$\phi = 5\%$, – $\phi = 10\%$, ····· $\phi = 20\%$.

achieved around $Gt = 8$ non-dimensional time units and slightly shorter for more concentrated suspensions. The third time scale T_{L1} allows the determination of the self-diffusion coefficients [see equation (18)]. The time integral of the autocorrelation function was found to be convergent for all concentrations. It defines the Lagrangian time scale $T_{Li} = \int_0^\infty R_{ii}(t)dt$ which increases with the concentration, since the negative loop is decreasing as ϕ increases. A summary of all these time scales is given in Table 1.

Shear Induced Self-Diffusion

If the particles experienced a pure Brownian motion, they would be subject to a short time self-diffusion related to the local instantaneous particle mobility. This diffusion would appear for a time scale longer than the relaxation time of the particle in the fluid and shorter than the time necessary to get uncorrelated motions. Another cause of diffusion would develop if the suspension had a concentration gradient. Then a 'collective' diffusion (Fick's law) would lead to a macroscopic migration of the particles. However, although the particles in this study are non-Brownian and the suspension is homogeneous, the loss of correlation after a long simulation time indicates that a self-diffusion behaviour develops in spite of the deterministic and linear nature of creeping flows. Indeed, the multi-body hydrodynamic interactions (Wang *et al.*, 1996) and the non-hydrodynamic repulsive forces lead to a fore-aft symmetry breaking, and induce the drift of the particles across the streamlines, enhancing the overall chaotic evolution of the suspension or the so-called shear-induced 'self-diffusion'. Transverse self-diffusion coefficients have been estimated by multiple approaches, but the determination of the diffusion coefficient in the flow direction is more complicated due to the combination of the diffusion and advection processes (Sierou and Brady, 2004). Acrivos *et al.* (1992) predicted theoretically the self-diffusion coefficient parallel to the flow by introducing a mechanism of interaction with an additional pair of particles. Sierou and Brady (2004) calculated this coefficient using a careful construction of the advection-diffusion namely the Fokker-Planck equation.

The transverse diffusion coefficient can be determined in two ways. Firstly, it can be evaluated from the integral of the velocity autocorrelation function over a long period of time [equation (18)].

$$D_{ii} = GT_{ii} \int_0^\infty R_{ii}(t)dt \qquad (18)$$

The self-diffusion coefficient is calculated in the shear and spanwise direction ($i = 2$ or 3) and it is scaled by Ga^2. It is the product of the fluctuation level times the Lagrangian integral time scale T_L which converges when the autocorrelation function tends to zero. It is important to note that we found in

Table 1. Correlation times versus concentration.

ϕ (%)	1	5	10	15	20
$G\ Tc_1$	1.16	1.18	1.16	1	1
$G\ Tc_2$	8.8	8.8	8.8	6.5	6.5
$G\ T_{L1}$	0.14	0.2	0.24	0.26	0.3

our simulations an enhancement of the velocity fluctuations but also an increase of the integral diffusion time with increasing concentration.

The second method is based on the long time behaviour of the particle mean-square displacement [equation (19)].

$$D_{ii} = \frac{1}{2\,Ga^2} \lim_{t\to\infty} \frac{d}{dt} \langle [x_i(t) - x_i(0)]^2 \rangle \tag{19}$$

In Figure 11 the temporal evolution of $<[x_i(t) - x_i(0)]^2>/t$ is plotted for suspension concentration ranging from 1 to 20%. This term has two different temporal regimes. It increases at short time and reaches at long times a plateau providing directly the diffusion coefficient. This representation of the time evolution of the mean square displacement is equivalent to the usual log-log representation used in the literature (Drazer et al., 2002; Marchioro and Acrivos, 2001; Sierou and Brady, 2004). At short time scales, the mean square displacement has a quadratic growth rate, i.e., its square root is linear and then the particle behaviour is not diffusive. The coefficient α [equation (20)] characterizes the mobility of the particles at short times.

$$\alpha_i = \frac{\sqrt{\langle [x_i(t) - x_i(0)]^2 \rangle}}{Gat} \tag{20}$$

The values of α_2 in Table 2 confirm that at short time scales the particle moves in the transverse directions with a typical velocity close to the particle averaged velocity fluctuation $\sqrt{T_{22}}$ (ballistic regime) in agreement with Taylor's theory on turbulent diffusion.

The growth of the transverse mean-square displacement is linear beyond the time necessary to reach uncorrelated velocity fluctuations. The diffusion coefficient D_{ii} is evaluated at long times, when the curves in Figure 11 reach a plateau. These curves show that the simulation times were long enough to reach the diffusion regime.

Transverse self-diffusion coefficients are strongly dependent on the volume fraction of the suspension [Figure 12(a) and (b)]. Da Cunha and Hinch (1996) and later Zarraga and
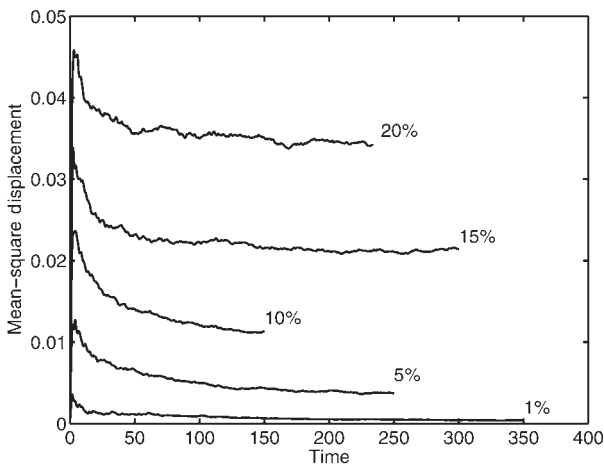
Figure 11. Temporal evolution of mean square displacement $<(x_2(t) - x_2(0))^2>/2\,Ga^2$ for different suspension concentrations. From bottom to top, the concentration is respectively 1, 5, 10, 15 and 20%.

Table 2. Comparison of the local mobility coefficient α_2 and the average velocity fluctuations in the shear direction.

ϕ (%)	1	5	10	15	20
α_2	0.0505	0.096	0.133	0.141	0.199
$(T_{22})^{1/2}$	0.0503	0.12	0.169	0.206	0.242

Leighton (2001) found that the shear-induced diffusion coefficient depends linearly on the concentration in the dilute regime. In their work, the particles are mainly driven by the non-hydrodynamic repulsive forces preventing particle overlap leading to a finite drift at each encounter. On the another hand, Wang et al. (1996) have shown theoretically that self-diffusion due to hydrodynamic interactions between more than two particles shows quadratic growth with concentration. Drazer et al. (2002) showed a transition between these two limiting behaviours when the strength of the repulsive force is substantially increased. The dependence of the
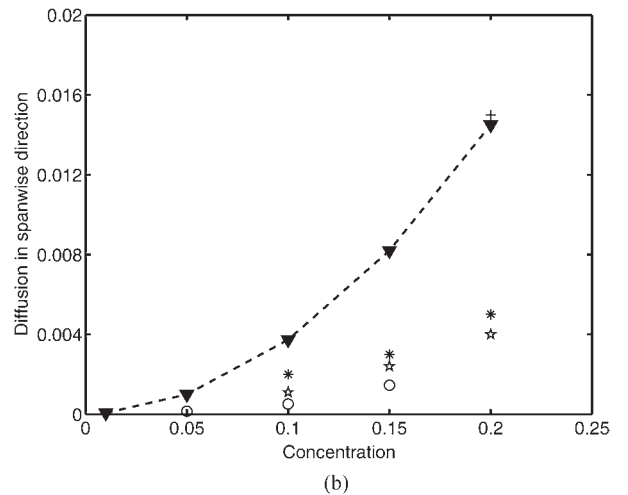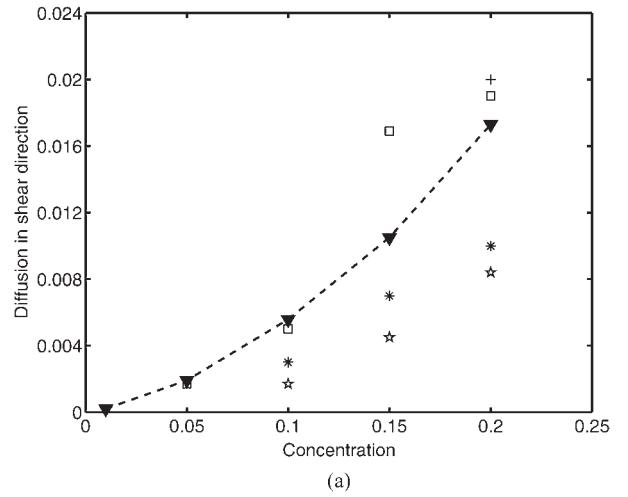
(a)

(b)

Figure 12. Evolution of the shear induced self-diffusion coefficient (a) in the shear direction D_{22} and (b) in the spanwise direction D_{33}. □ experimental work, Leighton and Acrivos (1986); +: experimental work, Breedveld et al. (2002); *: analytic work, Acrivos et al. (1992); o: Stokesian dynamics, Drazer et al. (2001); ☆: accelerated Stokesian dynamics: Sierou and Brady (2004); ▼ with dashed line: force coupling method simulations.

self-diffusion coefficient showed a cross over from a quadratic to linear scaling which is controlled by the finite drift across the streamlines induced by the non-hydrodynamic repulsive force. Our simulations show that the diffusion process does not depend only on the non-hydrodynamic effects, since the transverse self-diffusion coefficient does not scale linearly with the concentration. In an extremely dilute regime, we should recover this linear scaling but statistics take much longer time to converge as particle encounters become very rare. Thus, we have tested the effect of the repulsion barrier by varying the amplitude of the force scale at a constant concentration of the suspension. We obtain a scattering of less than 30% for large variations of the repulsion force. Compared to former studies, the self-diffusion coefficient computed with the FCM is slightly overestimated which is essentially related to the inaccurate representation of the local effects of viscous lubrication forces for small gap widths. When we improved the local hydrodynamic interactions by adding these lubrication forces (Abbas *et al.*, 2006), we noticed that the results obtained by simulations using the simple barrier repulsion are not completely misleading. The velocity fluctuation intensities and their PDF were well evaluated (with a 10% underestimation). The diffusion coefficient, which is in general more critical since it depends on the multi-body interactions and the final particle drift across the streamlines, was reduced to nearly 35% and had a fairly good agreement with the numerical work of Sierou and Brady (2004).

The self-diffusion tensor is anisotropic, i.e., $1.2 < D_{22}/D_{33} < 3$ for concentrations between 1 and 20%, recalling that the velocity fluctuations have the highest magnitude in the plane of the shear. High anisotropy of self-diffusion was also observed by Da Cunha and Hinch (1996) and Wang *et al.* (1996) for very dilute suspensions ($D_{22}/D_{33} \approx 10$). As we already mentioned, at low concentrations velocity fluctuations and consequently the self-diffusion coefficient are basically controlled by pair encounters which are highly anisotropic. When the concentration increases, multi-body hydrodynamic interactions enhance the fluctuations and diffusion of the particles in the direction perpendicular to the shear plane, and the ratios T_{33}/T_{22}, as well as D_{33}/D_{22}, are increasing (Figure 13). This trend is correct even for high concentrations up to 50% (Sierou and Brady 2004; Marchioro and Acrivos, 2001).

We conclude that the results obtained with the FCM are in the range of the former numerical and experimental investigations where data are scattered due to experimental uncertainties [a novel technique has been proposed by Breedveld *et al.* (1998)], simulation limitations (discussed in Sierou and Brady, 2004) and theoretical assumptions (Wang *et al.*, 1996).

CONCLUDING REMARKS AND PERSPECTIVES

The relation between macroscopic effective quantities and the microscopic structure of non-colloidal sheared suspensions under Stokes flow has been studied using the FCM. We considered that particles have the same density as the fluid and consequently we neglected inertia and buoyancy effects. Typical suspensions satisfying such conditions consist of solid micro-sized particles [$a = O(1 \, \mu m)$] suspended in a highly viscous liquid [$\nu = O(10^{-4} \, m^2 \, s^{-1})$]. Although these conditions are restrictive, such suspensions are of
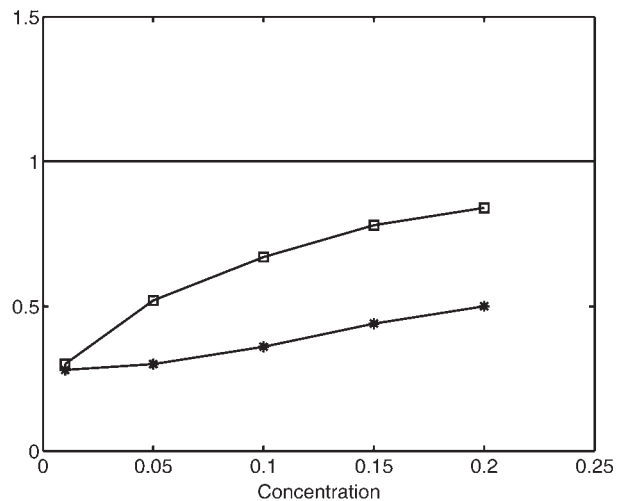

Figure 13. The evolution of anisotropy coefficients with concentration. Squares: D_{33}/D_{22}—Stars: T_{33}/T_{22}.

great interest in Chemical Engineering. The prediction of flows of suspension following oil extraction or conveying emulsions needs models accounting for multi-body hydrodynamic interactions. We chose the simple configuration of a pure linear shear flow as a prototype of interactions induced by local velocity gradients. In our simulations, fully periodic boundary conditions avoid segregation effects and the suspension remains homogeneous allowing the proper determination of statistics.

Interactions of particles occur because particles are moving on streamlines at different mean velocity and close interactions modifies the relative positions of the particle centres. The far field hydrodynamic interactions are well reproduced by the FCM. When the gap between the particle surfaces is very short, lubrication forces and non-hydrodynamic interactions may control the motion of particles. In a suspension stabilized by surfactants the interaction force is basically repulsive and can be approximated by DLVO-type forces where double layer electric repulsion overcomes the Van der Waals attraction. We were concerned with such suspensions where aggregation phenomena are negligible. The impact of these strong repulsive forces on the overall response of the suspension was previously found to be weak for moderately concentrated suspensions (20%), and its role has been discussed by Da Cunha and Hinch (1996) and Zarraga and Leighton (2000). The dynamics of stable suspensions have been well documented using different experimental and numerical methods (Breedveld *et al.*, 2002; Sierou and Brady, 2004; Drazer *et al.*, 2004).

After validating our numerical approach on simple systems of isolated or pairs of particles, we formed time averages on the trajectories of particles embedded in suspensions. The translational and rotational velocity fluctuations are found to be anisotropic and monotonically increasing in the range of solid volume fraction investigated. Particle pairs are formed even in static suspensions due to excluded volume effects, and their probability increases with concentration. When shearing the suspension for a long time the velocity fluctuations and the probability of finding close pairs of particles are enhanced. We found that the radial distribution of pairs close to contact is highly anisotropic. It is clearly related to

the repulsion force that prevents formation of pairs on the receding side of the test particle. Consequently, the T_{12} off-diagonal velocity fluctuation term is different from zero due to symmetry breaking of hydrodynamic interactions. The pairwise interactions played a dominant role at low concentrations. The shape of the probability distribution function of velocity fluctuations gradually evolves from Gaussian to exponential when the concentration decreases. Also, we observed that velocity autocorrelation functions have negative regions related to anticorrelation of velocity correlation on a time scale of order $1/G$ revealing that pair interactions are prominent. The velocity fluctuations remain correlated for a time of order $8/G$ before the lagrangian velocity autocorrelation function tends to zero. This loss of velocity correlation induced a hydrodynamic regime of diffusion. The shear-induced self-diffusion coefficients are determined in the transverse directions by two different methods showing that the results are consistent. We obtained a good agreement with previous numerical and experimental studies. The overall dynamics is well predicted by our numerical approach and this opens new fields of investigation.

The FCM is very flexible as we can implement very easily various potentials for interparticle forces. Brownian motion can also be modelled as a random force experienced by each particle leading to a prescribed diffusion behaviour. If interparticle forces are basically attractive, aggregation occurs and the kinetics of formation of clusters can be followed numerically. We successfully studied the formation kinetics of chains of paramagnetic particles (Climent *et al.*, 2004). We plan to use the same approach for seeking the stability of colloids when both Brownian motion and shear flow are simultaneously driving the motion of particles. Interaction potentials will be modelled using the DLVO theory with interparticle forces ranging from purely attraction to strong repulsion we already studied in the present paper.

NOMENCLATURE

a	particle radius, m
Ar:	Archimedes number
G	shear rate, s^{-1}
g	gravity constant, m s^2
k_B	Boltzman constant, J K^{-1}
Pe	Péclet number
Re	Reynolds number
St	Stokes number
T	fluid temperature, K
V	particle velocity, m s^{-1}
ρ_p	density of the particle, kg m^{-3}
ρ_f	density of the fluid, kg m^{-3}
μ_f	dynamic viscosity of the fluid, Pa s
ν_f	kinematic viscosity of the fluid, m s^{-2}

FCM

A, B and $C(r/a)$	hydrodynamic quantities
$A_{ij}^{(n)}$	anti-symmetric part of the dipole strength tensor N m^{-1}
$d^3\mathbf{x}$	elementary volume, m^3
$\mathbf{F}^{(n)}$	monopole force strength due to the nth particle, N
F_{ext}	external force on the center to the nth particle, N
F_b	repulsion barrier, N
$F_{ref}^{(n)}$	scale of the repulsion force, N
$G_{ij}^{(n)}$	dipole strength due to the nth particle, N m^{-1}
I_f	fluid inertia, kg m^{-2}
I_p	particle inertia, kg m^{-2}
L	width of the simulation domain, m

m_f	fluid mass, kg
m_p	particle mass, kg
p	pressure in the fluid, Pa
$\mathbf{r}$	separation distance between two particle centres, m
R_{ref}	cut-off distance of the repulsion barrier, m
$S_{ij}^{(n)}$	symmetric part of the dipole strength tensor, N m^{-1}
t	time, s
$T^{(n)}$	torque due to the nth particle, kg m^{-2} s^{-2}
$T_{ext}^{(n)}$	external torque, kg m^{-2} s^{-2}
$\mathbf{u}$	fluid velocity, m s^{-1}
$\mathbf{x}$	position in the fluid, m
$V^{(n)}$	velocity of the nth particle, m s^{-1}
$Y^{(n)}$	centre position of the nth particle, m
Δ and $\Delta'(x)$	Gaussian envelop of momentum source terms, m^{-3}
$\Omega^{(n)}$	particle rotation of the nth particle, rad s^{-1}
Λ	Hamaker constant, J
$\varepsilon_r \varepsilon_0$	fluid permittivity, C^2 J^{-1} m^{-1}
ψ	Electrical potential surface, V
σ and σ'	width of the Gaussian envelops, m

Suspension statistics

D_{ii}	shear induced self-diffusion coefficient tensor, dimensionless
$g(r)$	radial pair probability distribution function
G	shear rate
i	direction index−1: for the flow, 2: for the shear, 3: for the spanwise direction
n_i	particle number density
N	particle number inside the elementary volume $dV(r)$
R_{ii}	Lagrangian autocorrelation function of the velocity fluctuations
s	standard deviation of the velocity fluctuations, m s^{-1}
Tc_1, Tc_2, T_{Li}	autocorrelation time scales, s
T_{ij}	translational velocity fluctuation tensor, dimensionless
v_i	translational velocity fluctuation, m s^{-1}
w_{ij}	rotational velocity fluctuation tensor, dimensionless
$x_i(t)$:	particle position at time t, m
$x_i(0)$	particle position at the initial time, m
α_i	local mobility coefficient of the particles at short times
ϕ	suspension concentration
Γ_i	rotational velocity fluctuation, s^{-1}

REFERENCES

Abbas, M., Climent, E., Simonin, O. and Maxey, M.R., 2006, Dynamic of bidisperse suspensions under Stokes flows: Linear shear and sedimentation, accepted for publication in *Physics of Fluids*, 18: 121504/1−20.

Acrivos, A., Batchelor, G.K., Hinch, J., Koch, R. and Mauri, D.L., 1992, The longitudinal shear-induced diffusion of spheres in a dilute suspension, *J. Fluid Mech.*, 240: 651−657.

Allen, M.P. and Tildesley, D.J., 1987, Computer simulations of liquids (Oxford University Press, Oxford, UK).

Brady, J. and Bossis, G., 1985, The rheology of concentrated suspensions of spheres in simple shear flow by numerical simulation, *J Fluid Mech*, 155: 105−129.

Batchelor, G.K. and Green, J.T., 1972, The hydrodynamic interaction of two small freely-moving spheres in a linear flow field, *J Fluid Mech*, 56(2): 375−400.

Breedveld, V., Van den Ende, D., Tripathi, A. and Acrivos, A., 1998, The measurement of the shear-induced particle and fluid tracer diffusivities by a novel method, *J Fluid Mech*, 375: 297−318.

Breedveld, V., Van den Ende, D., Bosscher, M., Jongschaap, R.J.J. and Mellema, J., 2001, Measuring shear-induced self-diffusion in a counter-rotating geometry, *Phys Rev*, 63: 021403.

Breedveld, V., van den Ende, D., Bosscher, M., Fongschaap, R.J.J. and Mellema, J., 2002, Measurement of the full shear-induced

self-diffusion tensor of noncolloidal suspensions, *Journal of Chemical Physics*, 116: 10529−10535.

Climent, E., Maxey, M.R. and Karniadakis, G.E., 2004, Dynamics of self-assembled chaining in magneto-rheological fluids, *Langmuir*, 20: 507−513.

Dance, S.L., Climent, E. and Maxey, M.R., 2004, Collision barrier effects on the bulk flow in a random suspension, *Phys Fluids*, 16: 828−831.

Dance, S.L. and Maxey, M.R., 2003, Incorporation of the lubrication effects into the force- coupling method for particulate two-phase flow, *J Computational Physics*, 189: 212−238.

Da Cunha, F.R. and Hinch, E.J. 1996, Shear-induced dispersion in a dilute suspension of rough spheres, *J Fluid Mech*, 309: 211−223.

Drazer, G., Khusid, J.B. and Acrivos, A., 2002, Deterministic and stochastic behaviour of non-Brownian spheres in sheared suspensions, *J Fluid Mech*, 460: 307−335.

Drazer, G., Koplik, J., Khusid, B. and Acrivos, A., 2004, Microstructure and velocity fluctuations in sheared suspensions, *J Fluid Mech*, 511: 237−263.

Leighton, D. and Acrivos, A., 1986, Measurement of shear-induced self-diffusion in concentrated suspensions of spheres, *J Fluid Mech*, 177: 109−131.

Lomholt, S., Stenum, B. and Maxey, M.R., 2002, Experimental verification of the force coupling method for particulate flows, *Int J Multiphase Flows*, 28: 225−246.

Lomholt, S. and Maxey, M.R., 2003, Force-coupling method for particulate two-phase flow Stokes flow, *J Comp Phys*, 184: 381−405.

Marchioro, M. and Acrivos, A., 2001, Shear-induced particle diffusivities from numerical simulations, *J Fluid Mech*, 443: 101−128.

Maxey, M.R. and Patel, B.K., 2001, Localized force representations for particles sedimenting in Stokes flows, *Int J Multiphase Flow*, 27: 1603−1626.

Morris, J.F. and Kaytal, B., 2002, Microstructure from simulated Brownian suspension flows at large shear rate, *Phys Fluids*, 14: 1920−1937.

Rouyer, F., Martin, J. and Salin, D., 1999, Non Gaussian dynamics in quasi-2d non-colloidal suspension, *Phys Rev Lett*, 83, 1058−1061.

Sierou, A. and Brady, J.F., 2004, Shear-induced self-diffusion in non-colloidal suspensions, *J Fluid Mech*, 506: 285−314.

Verzicco, R. and Camussi, R., 2001, Structure function exponents and probability density function of the velocity difference in turbulence, *Physics of Fluids*, 14: 906−909.

Wang, Y., Mauri, R. and Acrivos., A., 1996, Transverse shear-induced liquid and particle tracer diffusivities of a dilute suspension of spheres undergoing a simple shear flow, *J Fluid Mech*, 327: 255−272.

Zarraga, I. and Leighton, D., 2001, Normal stress and diffusion in a dilute suspension of hard spheres undergoing simple shear, *Physics of Fluids*, 14: 565−577.

ACKNOWLEDGEMENTS